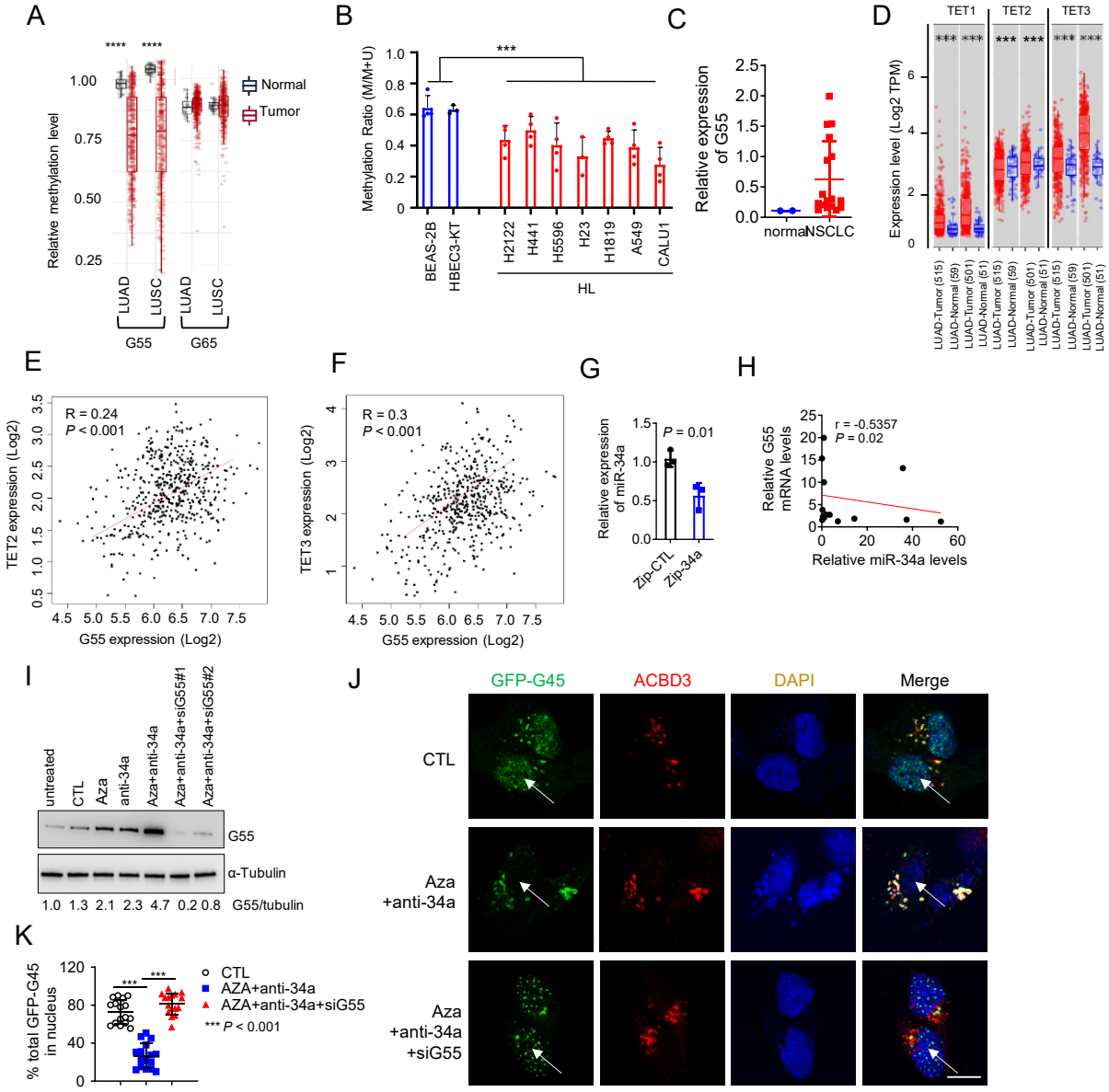
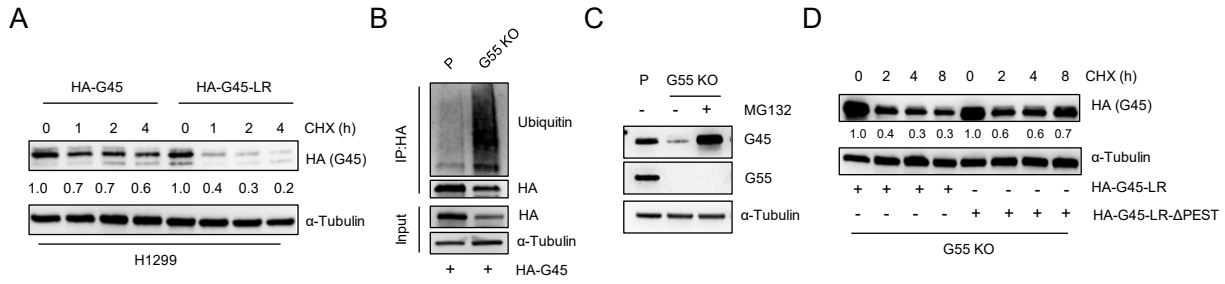
Supplemental Figures

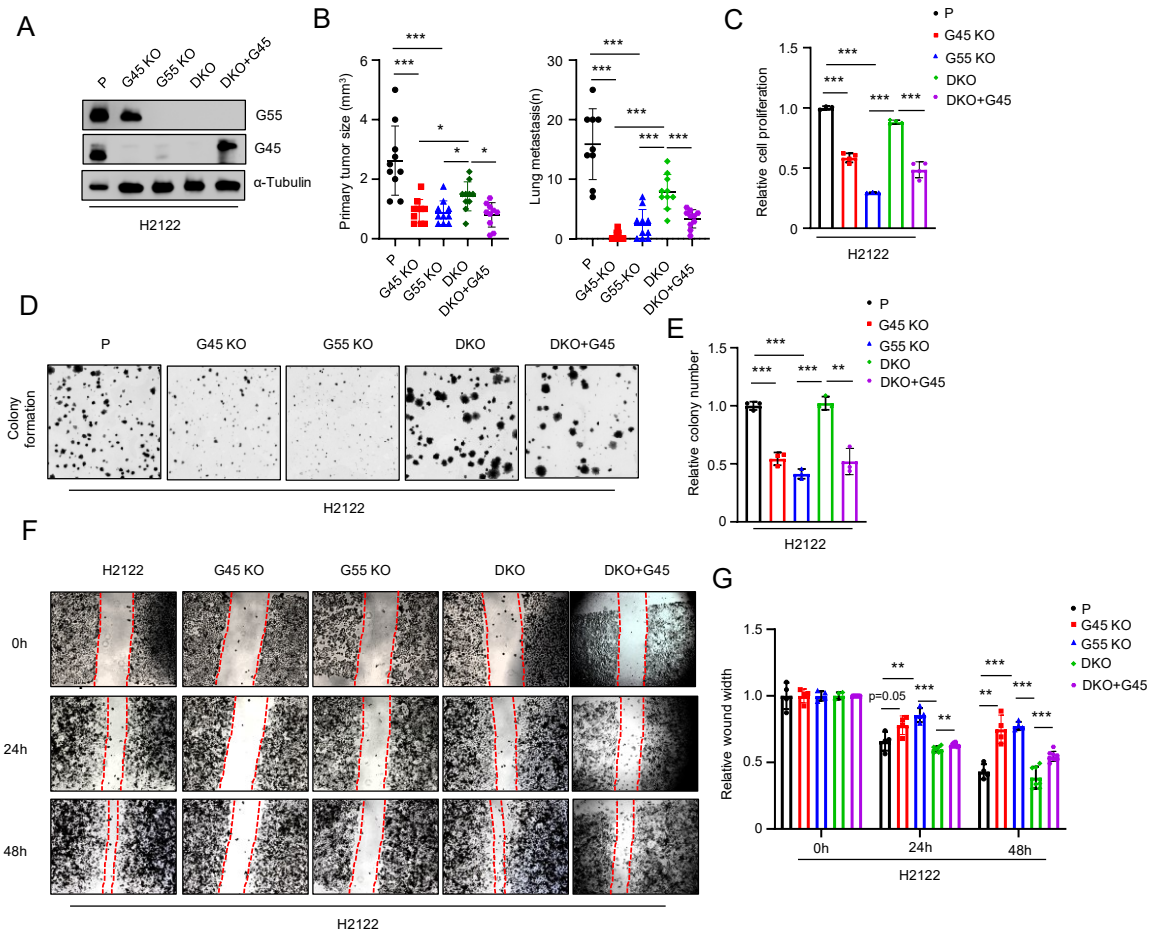


Supplemental Figure 1. Epigenetic upregulation of G55 in cancer. (A) Relative promoter methylation levels of GORASP2 (G55) and GORASP1 (G65) gene promoters in TCGA cohorts (LUAD, LUSC, and normal lung). (B) Ratios of methylated-to-unmethylated GORASP2 gene promoters in normal bronchial epithelial cells (blue) and lung cancer cell lines (red) determined by methylation-specific PCR. (C) qPCR analysis of G55 mRNA levels in normal bronchial epithelial (blue) and lung cancer cell lines (red). (D) Expression levels of DNA methylation regulators in normal lung (blue) or lung tumors (red). (E, F) Pearson correlation of G55 and TET2 (E) or TET3 (F) in the TCGA LUAD cohort. (G) qPCR confirmation of miR-34a knockdown in BEAS-2B cells transfected with plasmid expressing small RNA zippers targeting miR-34a (Zip-34a) or a control vector (Zip-CTL). (H) Pearson correlation of G55 mRNA and miR-34a levels in human lung cancer cell lines. (I) WB analysis of G55 protein levels in BEAS-2B cells treated,

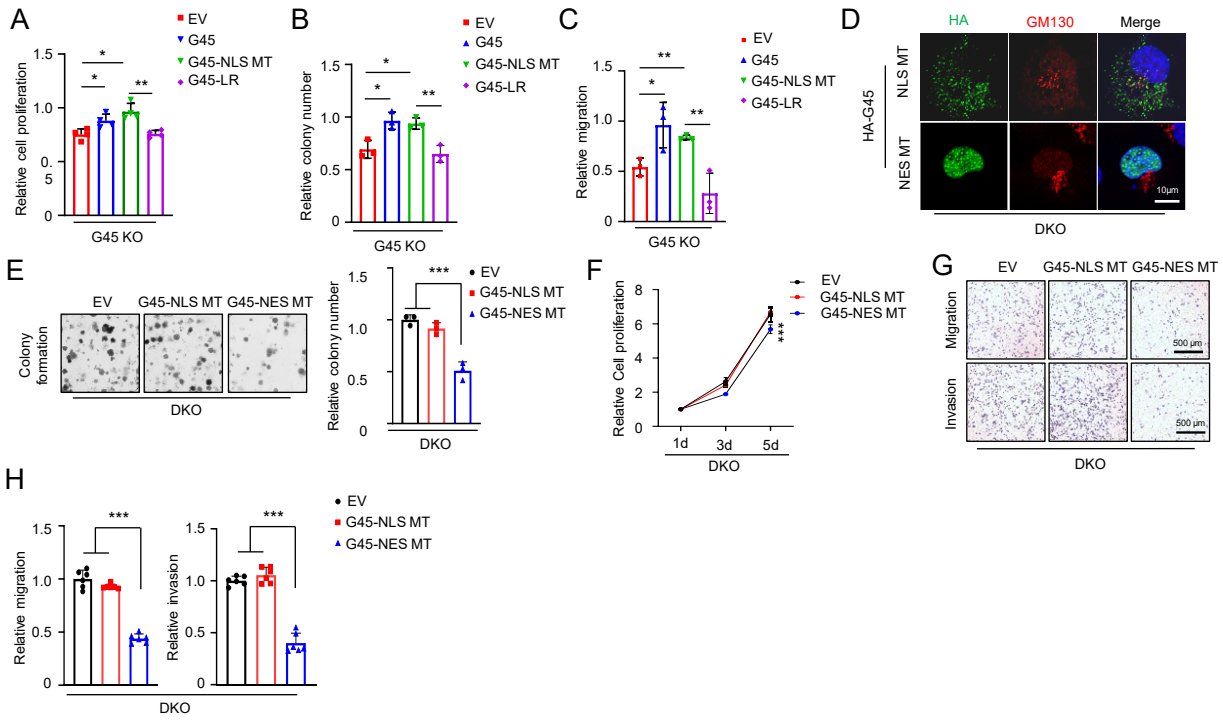
singly or in combination, with 5-Aza, miR-34a inhibitor, and G55 siRNA. Densitometric values relative to untreated cells. (J) Confocal micrographs of BEAS-2B cells transfected with a GFP-G45 expression vector and treated with 5-Aza and a miR-34a inhibitor, with or without G55 siRNA. Cells were immunostained with an ACBD3 antibody (red) and counterstained with DAPI (blue). (K) Percentage of total GFP-G45 in nuclei of BEAS-2B cells following indicated treatments. Data are presented as mean ± SD of triplicate samples. Arrows indicate nuclear G45 signals. Statistical analysis was performed using unpaired two-tailed t-test (B, C, D and G) or one-way ANOVA followed by Tukey's multiple comparisons test (K). $P < 0.05$ (*), $P < 0.01$ (**), and $P < 0.001$ (***).



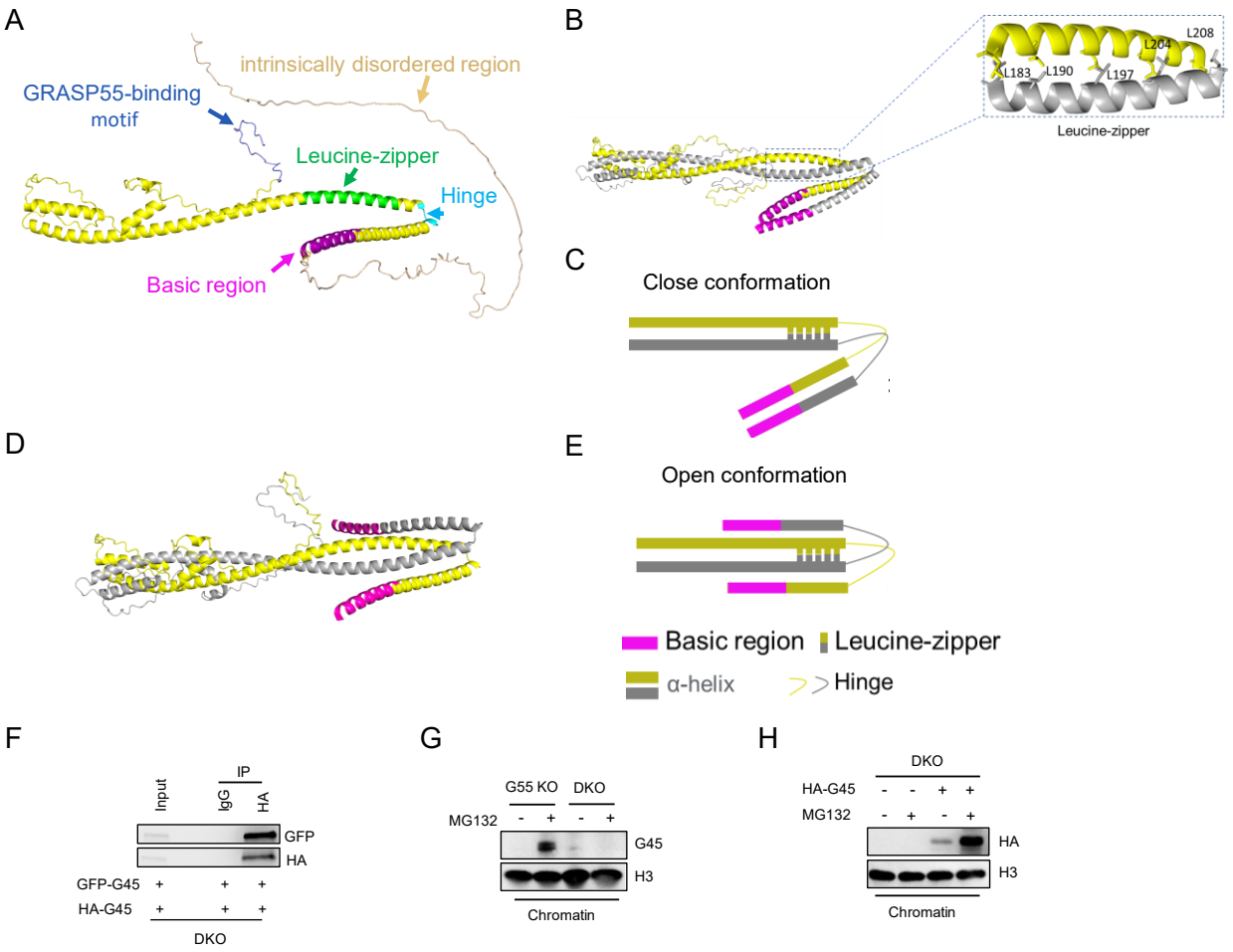
Supplemental Figure 2. Ubiquitin-mediated proteasomal degradation of nuclear G45. (A) WB analysis of H1299 cells transiently transfected with HA-tagged G45 constructs (WT or LR) and treated with cycloheximide (CHX) for different timepoints. (B) IP/WB analysis of HA-G45-transfected H1299 cells (P or G55 KO). Immunoprecipitated or total (input) proteins were blotted with anti-ubiquitin, -HA, or -tubulin antibodies. (C) WB analysis of endogenous G45 in G55 KO cells treated with (+) or without (-) MG132. (D) WB analysis of G55 KO cells transfected with LR with (ΔPEST) or without PEST domain deletion. Densitometric values relative to t=0. G55G55G55



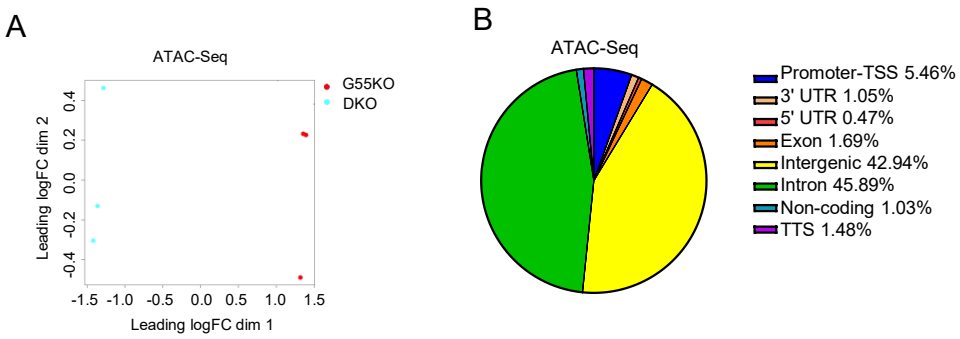
Supplemental Figure 3. Tumor suppressor activity of nuclear G45. (A) WB confirmation of gene targeting in H2122 cells. Tubulin loading control. (B) Primary tumor size (left plot) and metastases to contralateral lung (right plot) in mice (dots) bearing orthotopic lung tumors generated by cells in (A). (C) Relative densities of viable cells in monolayer culture. (D, E) Colonies generated by cells seeded at low density in monolayer culture were imaged (D) and quantified (E). (F, G) Images of scratch wounds taken at indicated timepoints (F) and quantified (G). Data are presented as mean ± SD of triplicate samples. Statistical analysis was performed using one-way ANOVA followed by Tukey's multiple comparisons test. $P < 0.05$ (*), $P < 0.01$ (**), and $P < 0.001$ (***).



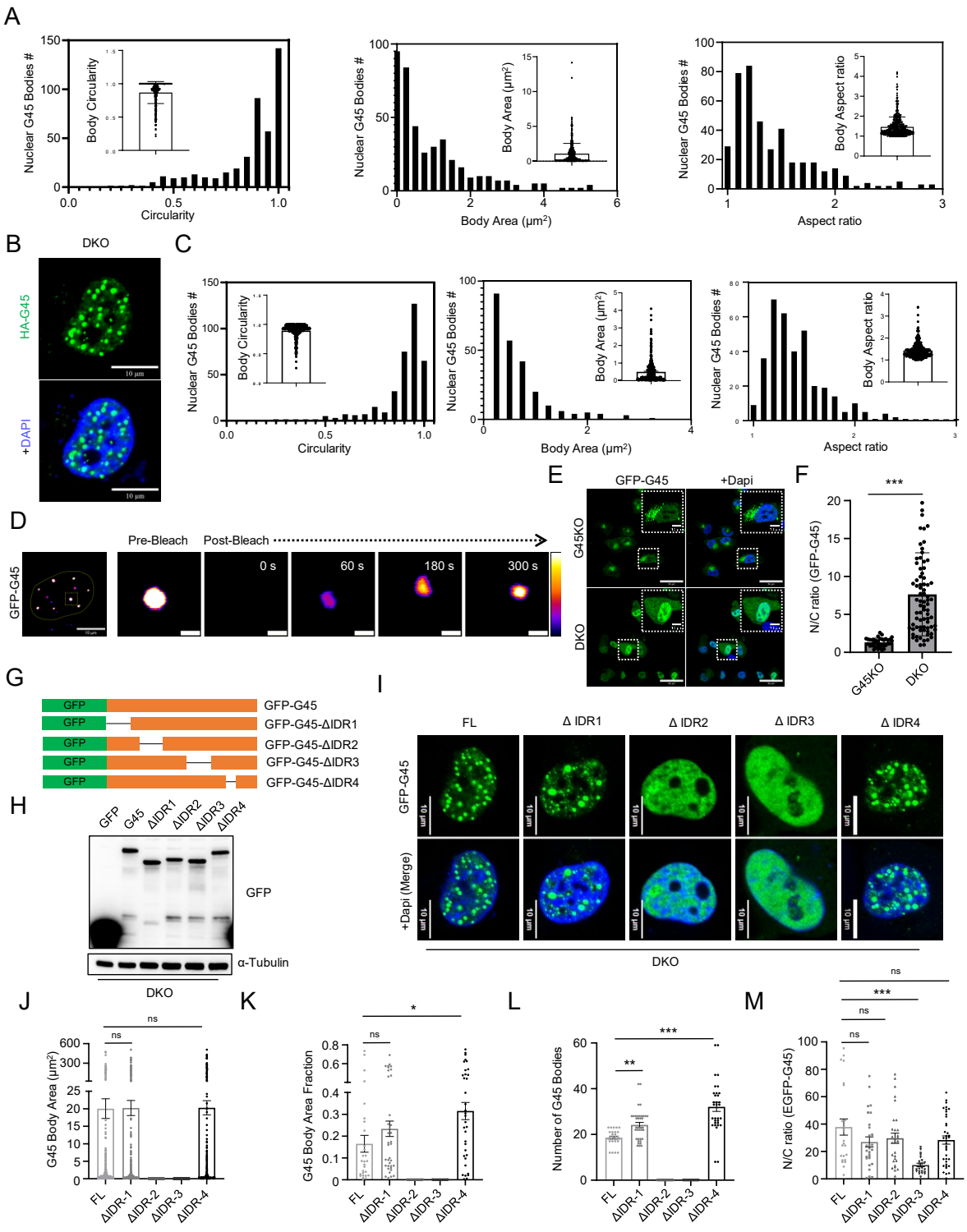
Supplemental Figure 4. Nuclear and Golgi-resident G45 exert opposing biological activities. (A-C) Viable cell density (A), colony formation (B), and migration (C) of G45 KO H1299 cells expressing EV, G45, G45-NLS MT, or G45-LR. (D) Confocal micrographs of DKO cells transfected with HA-tagged G45-NLS MT or G45-NES MT. (E) Colonies generated by DKO cells transfected with EV, HA-tagged G45-NLS MT or G45-NES MT seeded at low density in monolayer culture were imaged and quantified. (F) Densities of viable DKO cells in monolayer culture. (G, H) Migrated and invaded cells in Boyden chambers were photographed (G) and quantified (H). Data are presented as mean ± SD of triplicate samples. Statistical analysis was performed using one-way ANOVA followed by Tukey's multiple comparisons test. $P < 0.05$ (*), $P < 0.01$ (**), and $P < 0.001$ (***).



Supplemental Figure 5. Structural modeling of G45. (A) G45 domain structure by AlphaFold. N-terminal intrinsically disordered region (wheat), basic region (purple), hinge (cyan), Leucine-zipper (green), and G55-binding motif (slate). (B-E) G45 dimer in closed (B, C) and open (D, E) conformations. In both conformations, G45 dimer is locked together by 5 leucine pairs in the Leucine-zipper motif. Leucine residues in the closed conformation highlighted (inset, B). In the closed conformation, the Basic regions (purple) of two G45 subunits are brought together, whereas in the open conformation, they are separated. (C, E) Schematics showing G45 dimer in closed (C) and open (E) conformations. Since the Basic regions in Leucine-zipper proteins are known to interact with the acidic phosphate moieties of DNA, our models suggest that G45 Basic regions (purple) may function similarly to the two arms of tongs, facilitating the gripping of DNA. (F) IP/WB analysis of co-transfected (HA-G45 + GFP-G45) DKO cells. Anti-HA- or IgG-immunoprecipitated proteins were blotted with anti-GFP or anti-HA antibodies. (G, H) WB analysis of endogenous G45 (G) or HA-G45 (H) in chromatin preparations from cells treated with (+) or without (-) MG132 proteasomal inhibitor. H3 histone loading control.

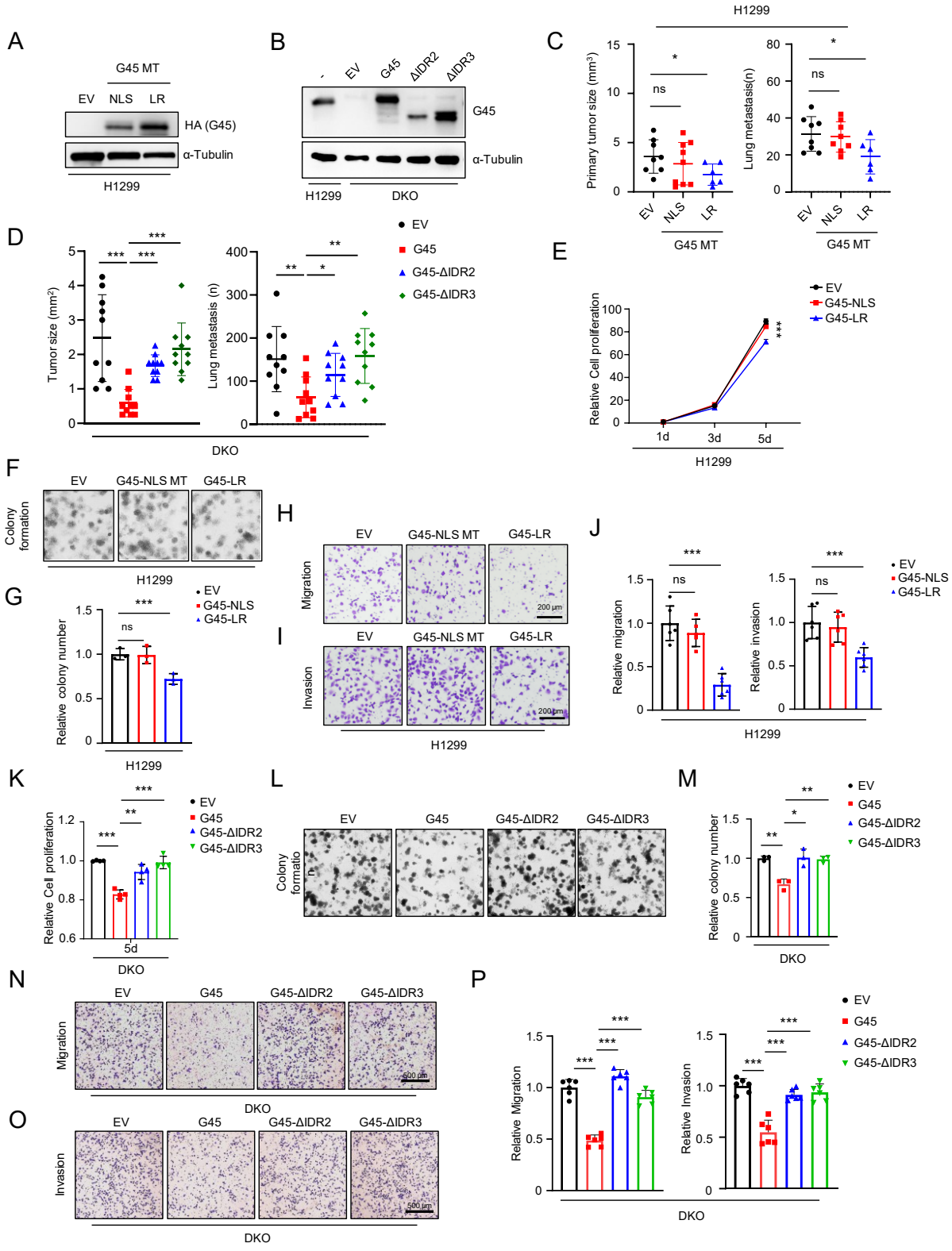


Supplemental Figure 6. Nuclear G45-regulated chromatin accessibility changes. (A) Principal component analysis (PCA) of samples analyzed by ATAC-seq (G55 KO versus DKO, n=3 per condition). (B) Pie chart illustrates genomic regions with differences in chromatin accessibility.



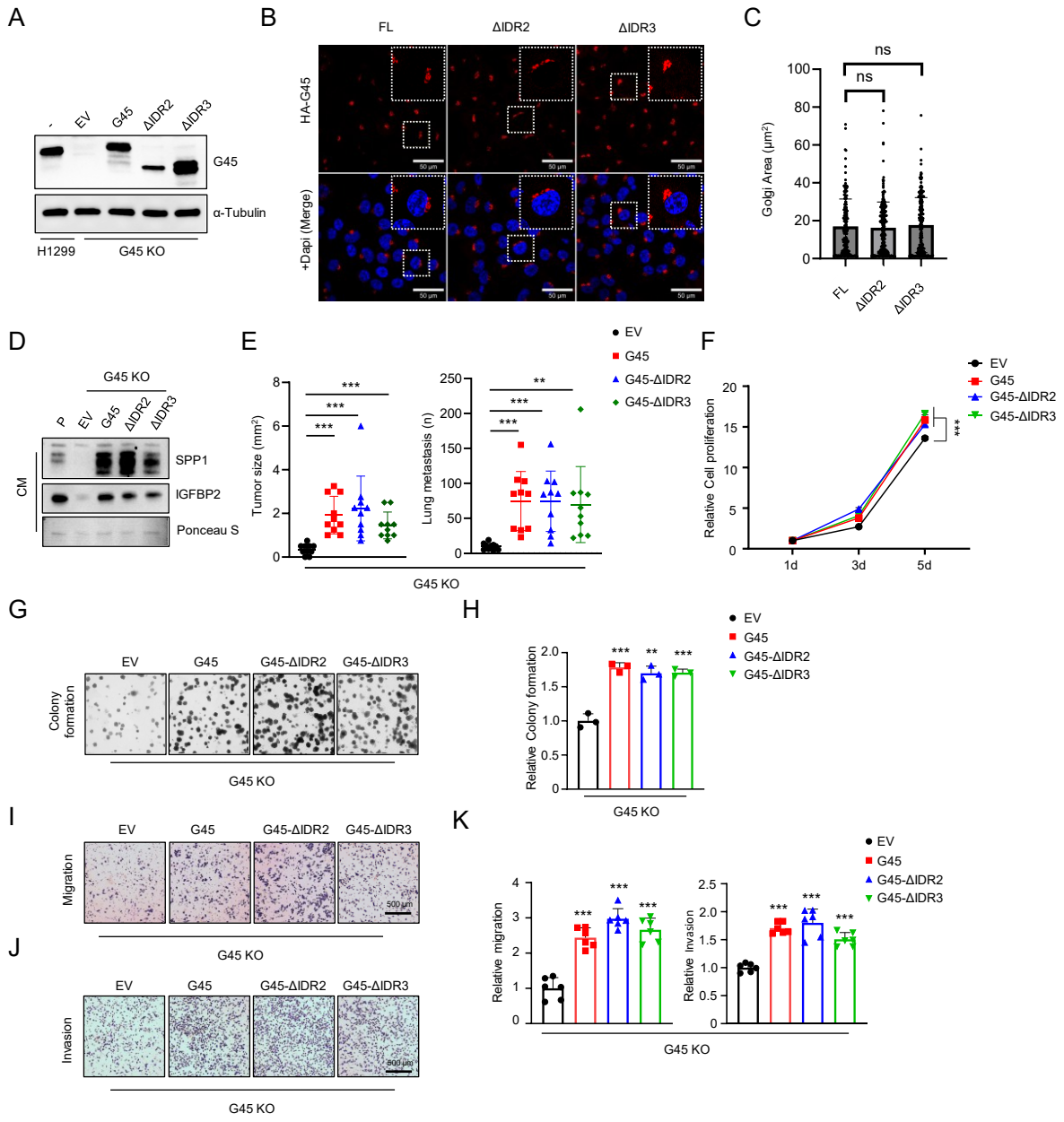
Supplemental Figure 7. LLPS-generated G45 nuclear bodies require IDR2 and IDR3. (A) Body circularity (left plot), areas (middle plot), and aspect ratios in EGFP-G45-transfected H1299 cells. n = 426 bodies. (B, C) Representative confocal images showing HA-G45 nuclear bodies in DKO cells (B). Body circularity (left plot), areas (middle plot), and aspect ratios in HA-G45-

transfected DKO cells were quantified (C). Scale bar, 10 μm. (D) Confocal micrographs of EGFP-G45-transfected H1299 cells before (pre-) and after (post-) bleaching. Regions of interest in far-left panels (boxes) shown at higher magnification at different timepoints. (E, F) Confocal micrographs of EGFP-G45-transfected cells (E). EGFP signal expressed as N/C ratio per cell (F). n = 36 and 78 cells for G45KO and DKO, respectively. (G) Schematic of full-length (GFP-G45) or IDR-deleted (ΔIDR1-4) constructs. (H) WB confirmation of GFP-tagged full-length and IDR-truncated G45 expression in DKO cells. (I) Single-channel and merged confocal micrographs of EGFP-G45-transfected DKO cells. (J-M) Body areas (J), body area fractions (K), body numbers (L), and G45 N/C ratios (M) per cell from (I). n = 500-1000 bodies from 20-40 cells for full-length G45 or the different IDR-deleted (∆ IDR1 – 4) mutants. Error bars = SEM. Statistical analysis was performed using unpaired two-tailed t-test (F) or one-way ANOVA followed by Tukey's multiple comparisons test (J-M). $P < 0.05$ (*), $P < 0.01$ (**), and $P < 0.001$ (***).



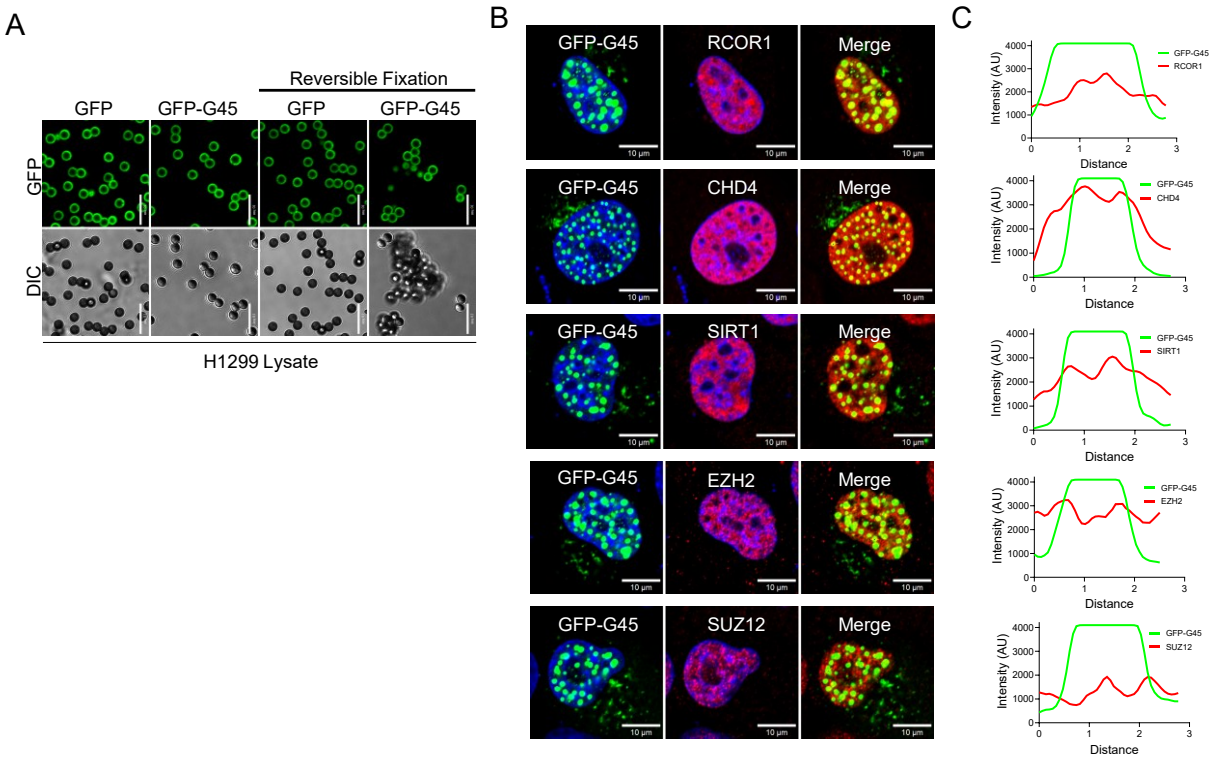
Supplemental Figure 8. Tumor suppressor activity requires NLS and IDRs on G45. (A, B) WB analysis of parental H1299 cells stably transfected with HA-tagged LR or nuclear localization site (NLS)-mutant G45 (A) or DKO cells stably transfected with HA-tagged WT, IDR2-, or IDR3-

deficient G45 (B). (C) Primary tumor size (left plot) and metastases to contralateral lung (right plot) in mice (dots) bearing orthotopic lung tumors generated by cells in (A). (D) Primary tumor size (left plot) and metastases to contralateral lung (right plot) in mice (dots) bearing orthotopic lung tumors generated by cells in (B). (E) Densities of viable H1299 cells in monolayer culture. Empty vector (EV). (F, G) Colonies at low density monolayer culture were photographed (F) and quantified (G). (H-J) Migrated (H) and invaded (I) cells in Boyden chambers were photographed and quantified (J). (K) Densities of viable DKO cells stably expressing EV, G45, G45-ΔIDR2, or G45-ΔIDR3 in monolayer culture. (L, M) Colonies in low-density monolayer culture were photographed (L) and quantified (M). (N-P) Migrated (N) and invaded (O) cells in Boyden chambers were photographed and quantified (P). Data are presented as mean ± SD of triplicate samples. Statistical analysis was performed using one-way ANOVA followed by Tukey's multiple comparisons test. $P < 0.05$ (*), $P < 0.01$ (**), and $P < 0.001$ (***).

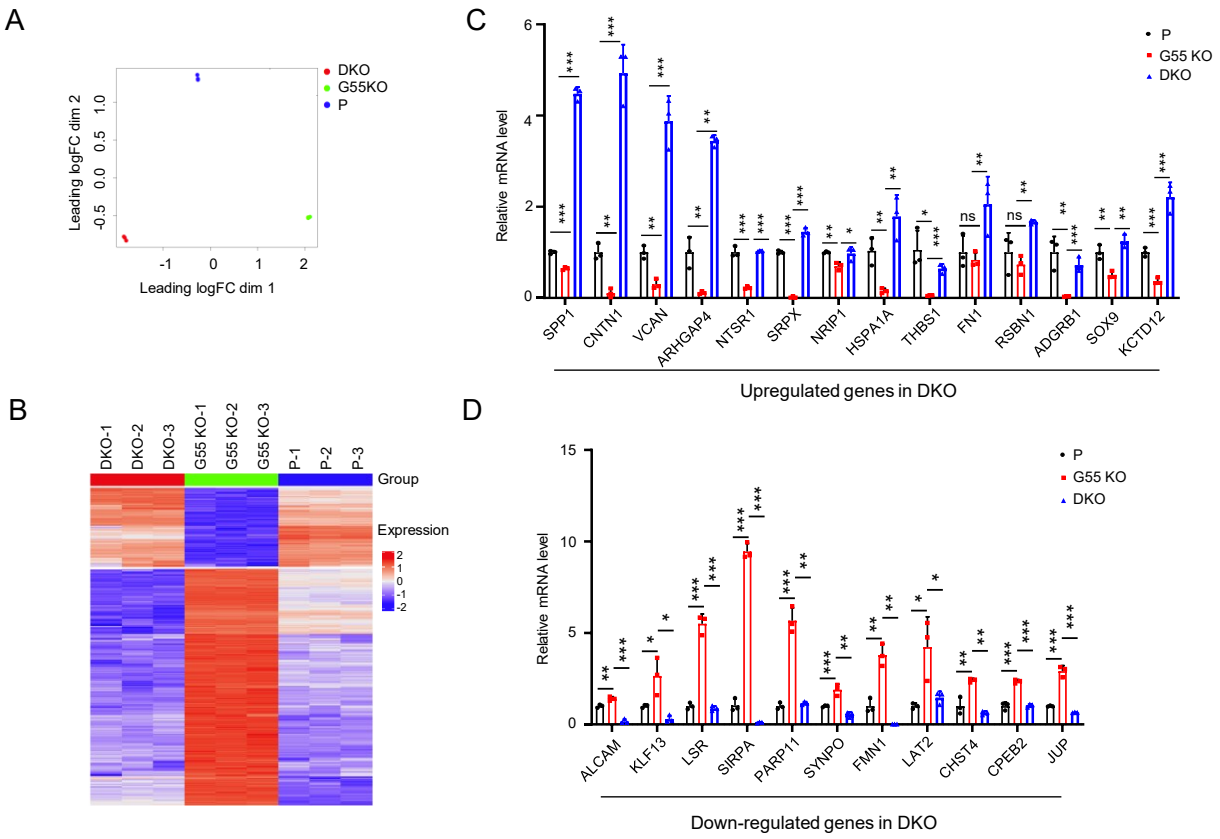


Supplemental Figure 9. IDRs are not required for Golgi-resident G45's pro-tumorigenic activity. (A) WB confirmation of ectopic G45 expression in G45 KO H1299 cells. HA-tagged WT G45 (G45) or IDR-deficient G45 (ΔIDR). Tubulin loading control. (B) IF analysis of HA-tagged WT G45 (FL, n=180 cells), G45-ΔIDR2 (n=232 cells), and G45-ΔIDR3 (n=216 cells) in G45 KO H1299 cells. (C) Golgi area per cell (dot) demonstrates no measurable differences between groups in (B). (D) WB analysis of known G45-regulated secreted proteins (1) in CM samples from G45 KO H1299 cells reconstituted with empty vector (EV) or WT (G45) or IDR-deficient (ΔIDR) G45. Ponceau S loading control. (E) Primary tumor size (left plot) and metastases to contralateral lung (right plot) in mice (dots) bearing orthotopic lung tumors generated by cells in (A). (F) Densities of viable cells in monolayer culture. (G, H) Colonies generated by cells seeded at low density in monolayer culture were imaged (G) and quantified (H). Results expressed relative to EV. (I-K) Migrated (I)

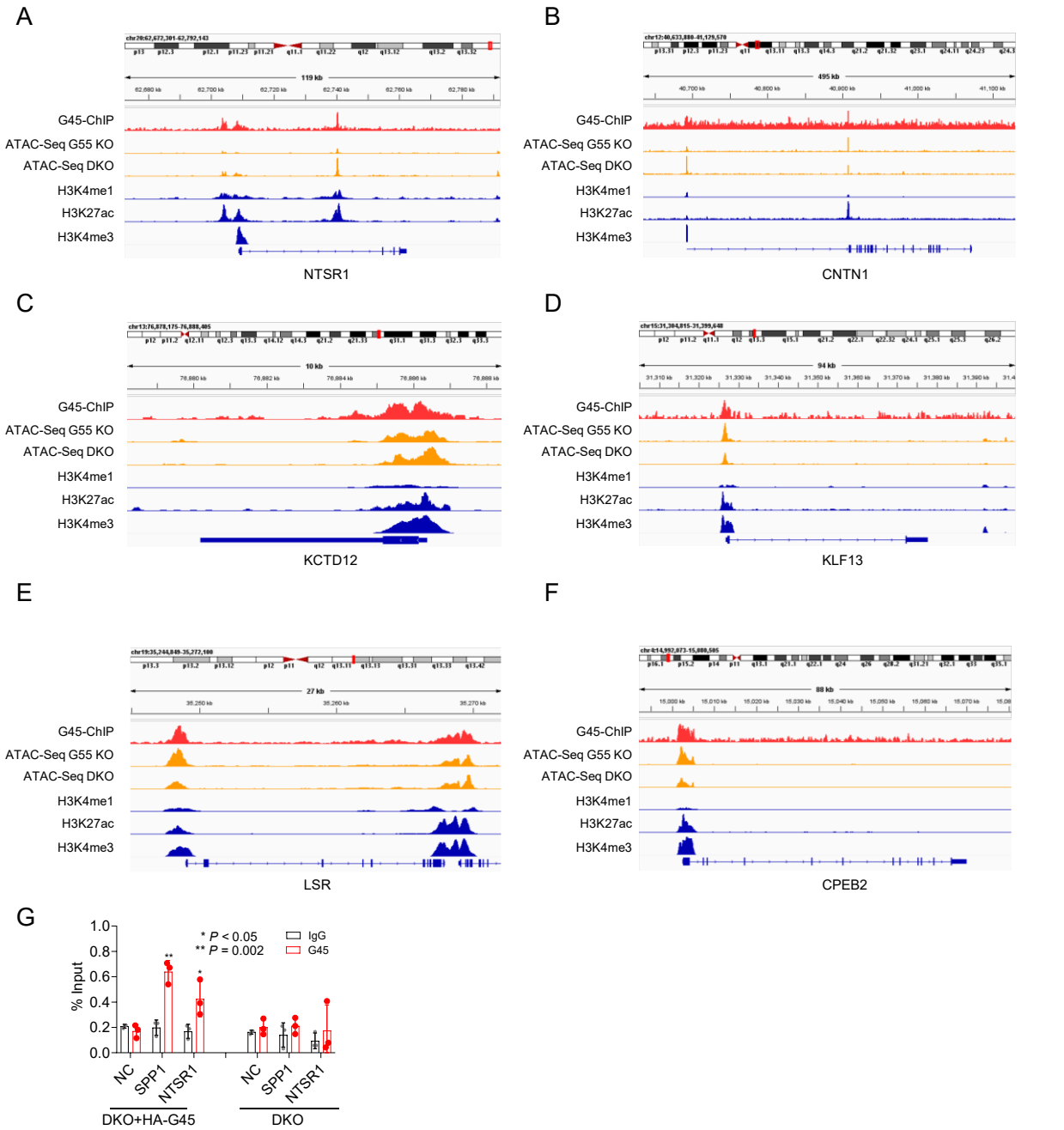
and invaded (J) cells in Boyden chamber assays were imaged and quantified (K). Results expressed relative to EV. Data are presented as mean ± SD of triplicate samples. Statistical analysis was performed using one-way ANOVA followed by Tukey's multiple comparisons test. $P < 0.01$ (**) and $P < 0.001$ (***).



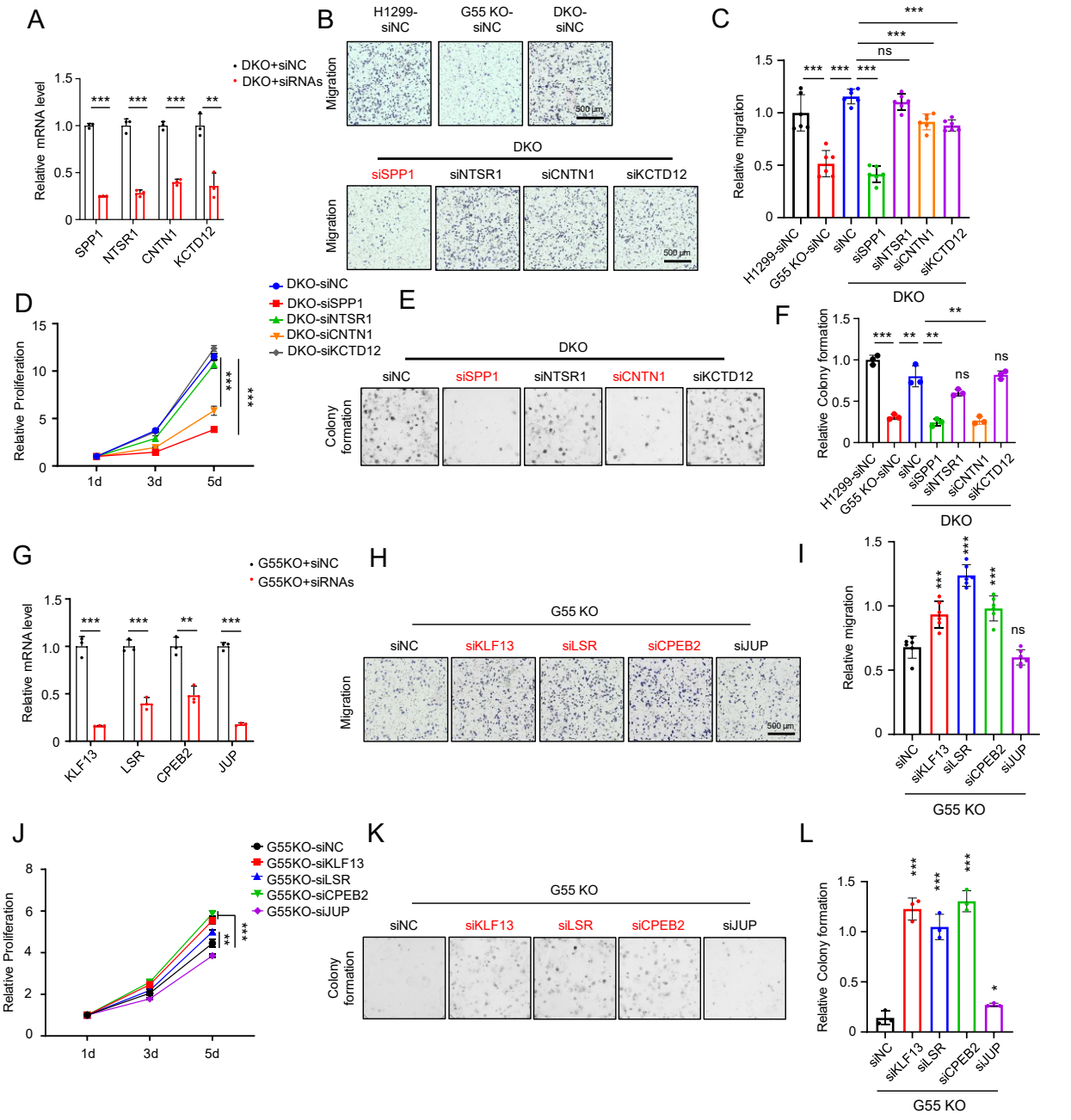
Supplemental Figure 10. Transcriptional repressors in G45 bodies. (A) Fluorescence (upper panels) and differential interference contrast (DIC) microscopy of bodies in H1299 cells that had or had not undergone reversible fixation. Body coalescence observed in fixed conditions is consistent with protein cross-linking. (B, C) Confocal micrographs of transcriptional repressors RCOR1, CHD4, SIRT1, EZH2, and SUZ12 in G45 bodies (B) and corresponding intensity line profiles showing colocalization with G45 (C).



Supplemental Figure 11. A nuclear G45-regulated transcriptome. (A, B) Principal component analysis (A) and heat map representation (B) of RNA-seq data from total cellular RNA samples (n=3 replicates per condition). (C, D) qPCR confirmation of genes found to be upregulated (C) or downregulated (D) in DKO cells relative to G55 KO cells. Data are presented as mean ± SD of triplicate samples. Statistical analysis was performed using one-way ANOVA followed by Tukey's multiple comparisons test. $P < 0.05$ (*), $P < 0.01$ (**), and $P < 0.001$ (***).

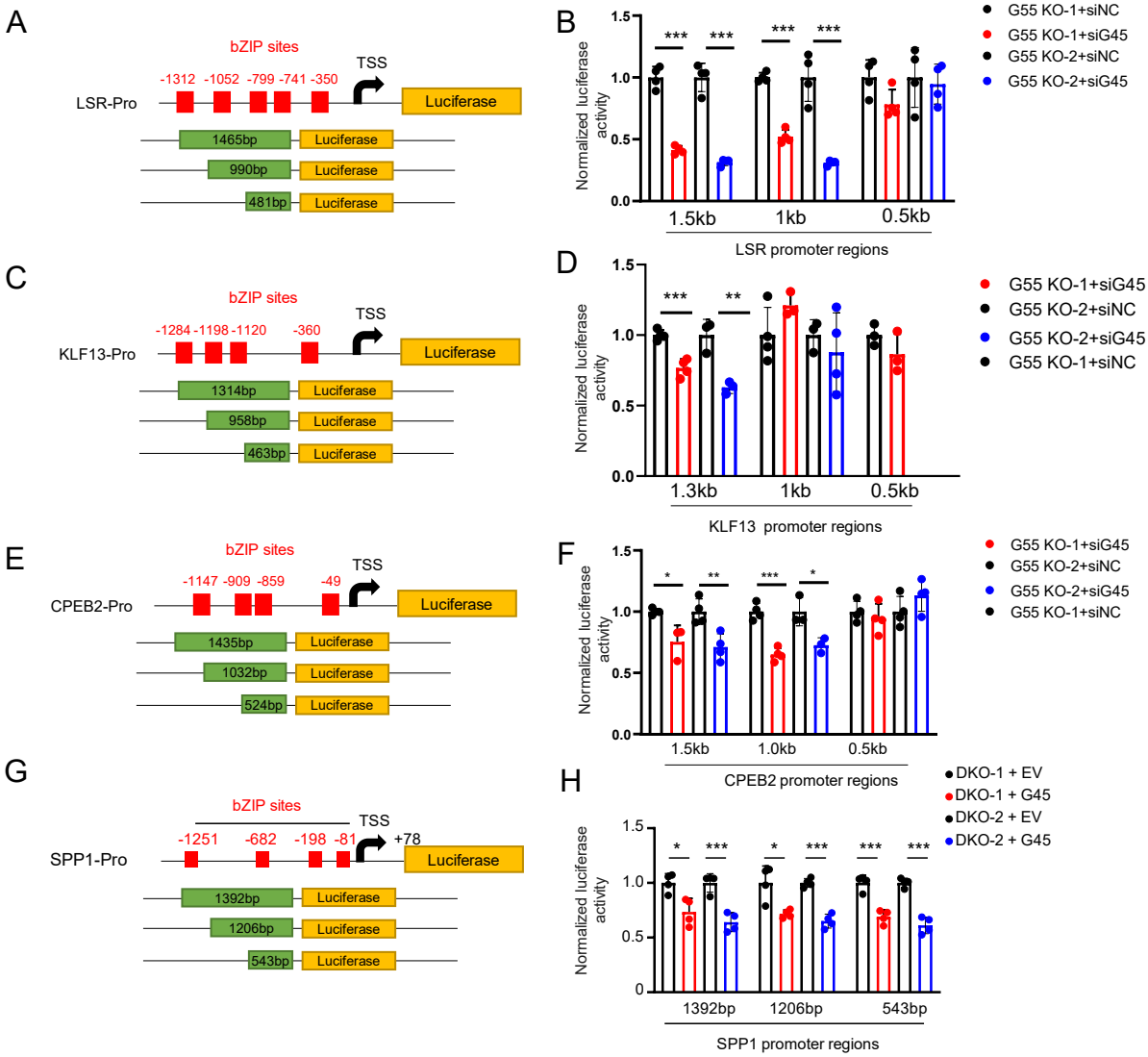


Supplemental Figure 12. Nuclear G45 target genes. (A-F) Schematic representation of G45-ChIP and ATAC-seq in genes that were downregulated (A-C) or upregulated (D-F) by nuclear G45. For G45-ChIP, DKO cells were transfected with HA-G45 and immunoprecipitated with anti-G45 antibody. ATAC-seq was performed using H1299 G55 KO and G45/G55 DKO cells. Findings were aligned with reported H3K4me1, H3K4me3, and H3K27ac ChIP-seq data (2). (G) ChIP-qPCR confirmation of nuclear G45 target genes in DKO cells transfected with or without HA-G45 and immunoprecipitated with anti-G45. Data are presented as mean ± SD of triplicate samples. Statistical analysis was performed using unpaired two-tailed t-test.

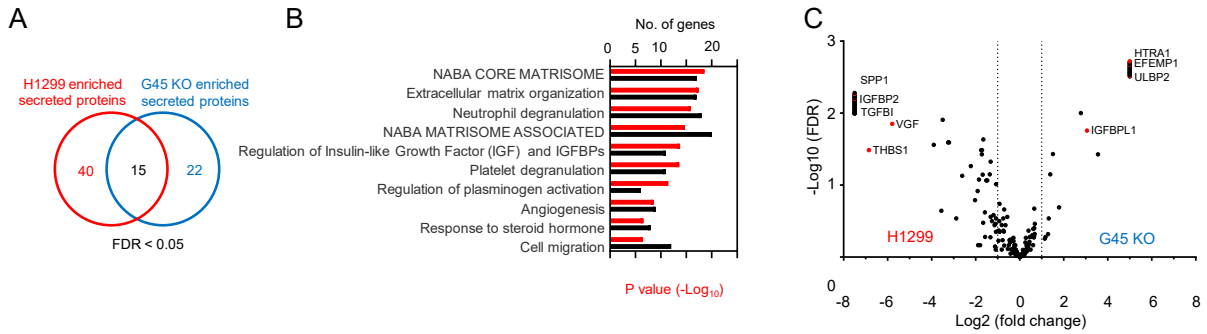


Supplemental Figure 13. Functional screens of G45 target genes. (A-F) Downregulated G45 target genes. qPCR confirmation of siRNA-mediated target gene knockdown in DKO cells (A). Migrated cells in Boyden chambers were photographed (B) and quantified (C). Viable cells in monolayer culture were quantified at distinct timepoints (D). Colonies formed at low density in monolayer culture were photographed (E) and quantified (F). (G-L) Upregulated G45 target genes. qPCR confirmation of siRNA-mediated target gene knockdown in G55 KO cells (G). Migrated cells in Boyden chambers were photographed (H) and quantified (I). Viable cells in monolayer culture were quantified at distinct timepoints (J). Colonies formed at low density in monolayer culture were photographed (K) and quantified (L). Data are presented as mean ± SD of triplicate samples. Statistical analysis was performed using unpaired two-tailed t-test (A and G)

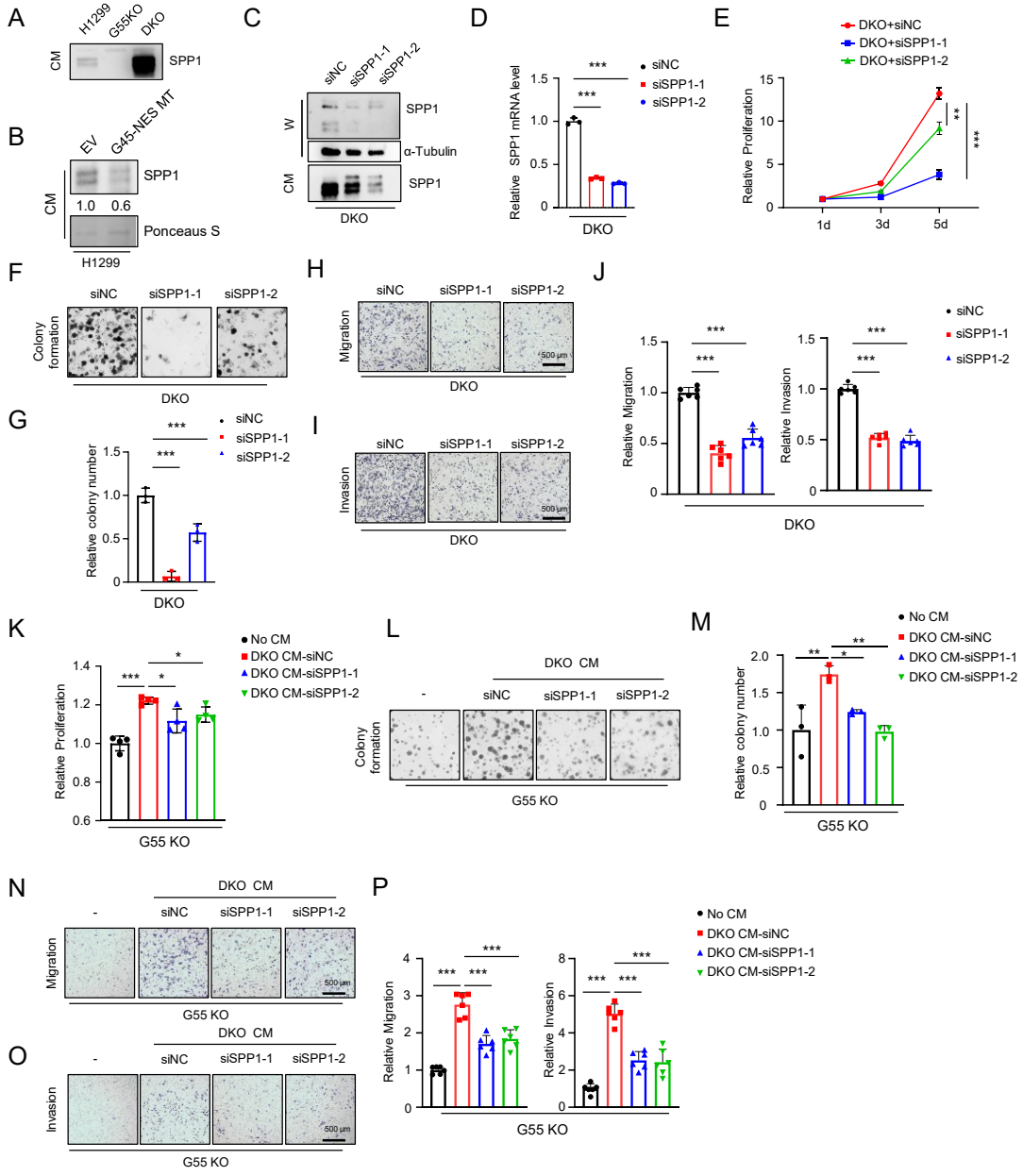
or one-way ANOVA followed by Tukey's multiple comparisons test (C, D, F, I, J and L). $P < 0.05$ (*), $P < 0.01$ (**), and $P < 0.001$ (***).



Supplemental Figure 14. Nuclear G45 regulates target gene promoter activity. (A–H) Schematic representation of luciferase reporter constructs containing the indicated promoter regions and predicted bZIP-binding sites of the G45 target genes LSR, KLF13, CPEB2, and SPP1 (A, C, E, G), and corresponding luciferase reporter assays following G45 knockdown in G55-KO cells (B, D, F, H). Data are presented as mean ± SD, with individual biological replicates shown as dots. Statistical analysis was performed using an unpaired two-tailed t test. P < 0.05 (*), P < 0.01 (**), and P < 0.001 (***).

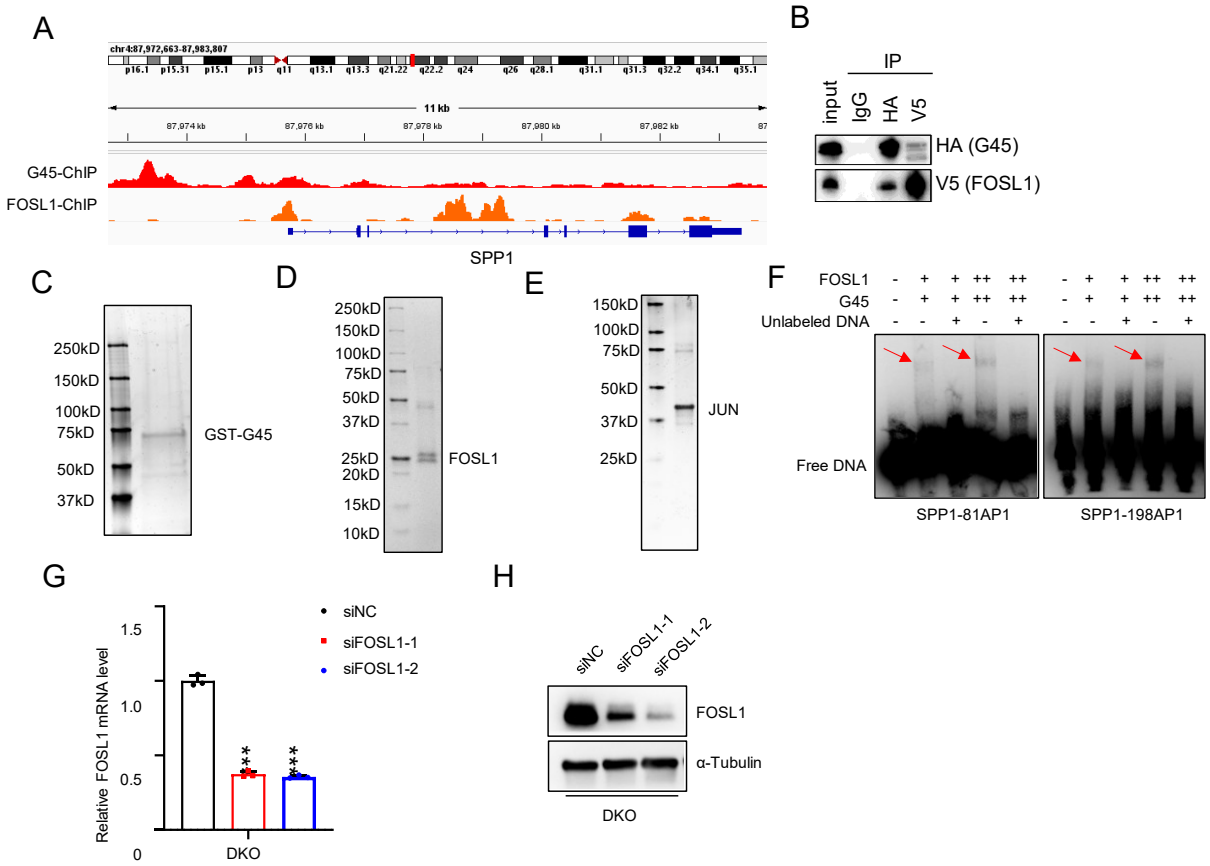


Supplemental Figure 15. G45 regulates the secretome. (A) Venn diagram showing secreted proteins identified by mass spectrometry analysis of CM samples from parental and G45-KO H1299 cells. (B) GO term enrichment analysis of secreted proteins that are differentially abundant in the CM of parental and G45-KO H1299 cells. (C) Volcano plot showing the identified secreted proteins.



Supplemental Figure 16. Nuclear G45 decreases SPP1 secretion, a pro-tumorigenic effector. (A) WB analysis of SPP1 in CM samples. (B) WB analysis of SPP1 in CM samples from H1299 cells overexpressing G45 NES-MT or EV. (C, D) WB (C) and qPCR (D) confirmation of siRNA-mediated gene knockdown. Whole cell lysate (W). (E) Viable cells in monolayer culture were quantified at distinct timepoints. (F, G) Numbers of colonies formed at low density were imaged (F) and quantified (G). (H-J) Relative numbers of migrated and invaded cells in Boyden chambers (H, I) were quantified in (J). Results expressed relative to siNC control. (K) Relative densities of cells in monoculture. (L, M) Colonies in low density monolayer culture were photographed (L) and expressed relative to control (M). (N-P) Boyden chamber assays of migrated and invaded cells were photographed (N, O) and quantified (P). Data are presented as mean ± SD of triplicate

samples Statistical analysis was performed using one-way ANOVA followed by Tukey's multiple comparisons test. $P < 0.05$ (*), $P < 0.01$ (**), and $P < 0.001$ (***).



Supplemental Figure 17. Target gene silencing by nuclear G45. (A) Schematic view across the SPP1 gene locus with genomic information. G45-ChIP in DKO cells. FOSL1-ChIP in DU145 cells (3). (B) IP/WB analysis on G55 KO cells co-transfected with HA-tagged G45 and V5-tagged FosL1 expression constructs. Lysates were immunoprecipitated with anti-HA, anti-V5, or IgG, and WB analysis was carried out on immunoprecipitated proteins or cell lysates (input). (C-E) SDS-PAGE confirmation of intact recombinant proteins. GST-G45 (C), His-tagged FOSL1 (D), and His-tagged JUN (E) proteins. (F) Electrophoretic mobility shift assays using labeled ± unlabeled SPP1 promoter regions (50bp with bZIP-binding sites at −81 bp or −198). Binding activity of FOSL1 and G45 proteins was competed by unlabeled DNA. Red arrows indicate the specific shifted band. (G, H) qPCR (G) and WB blot (H) confirmation of target gene knockdown in DKO cells transfected with FOSL1 siRNA or control siRNA. Data are presented as mean ± SD of triplicate samples. Statistical analysis was performed using unpaired two-tailed t-test. $P < 0.05$ (*), $P < 0.01$ (**), and $P < 0.001$ (***).

Supplemental Methods

Isolation and characterization of G45 nuclear bodies. G45 nuclear bodies were isolated essentially as described(4). Briefly, H1299 cells transfected with either control EGFP or EGFP-G45 or IDR deleted EGFP-G45 using jetPRIME reagent according to the manufacturer's protocol and were harvested after 30 h by trypsinization after checking the transfection efficiency (~60%). Cells were counted and ~ 45 million cells were pelleted in 15ml tube followed by washing with PBS and pellets frozen at –80 °C, then thawed on ice and lysed in ice-cold 200 µl lysis buffer (1% NP-40 (Sigma Aldrich) in DPBS (Thermo Fisher Scientific)), 4 µl protease and phosphatase inhibitor (Thermo Fisher Scientific) and 10 µl RNaseout (Thermo Fisher Scientific) for 30 min on ice with intermittent vortexing. Lysates were spun at 220g for 5 min, 4 °C and transferred to a new Eppendorf tube and sonicated for 25 pulses (1 s by 1 s square pulse at 30% amplitude). Lysates were spun at 5000 g for 30 min at 4 °C to remove cellular debris. To further clarify, the supernatant was transferred to a new Eppendorf tube and spun again at 5000 g for 10 min at 4 °C. Simultaneously, 120 µl GFP trap Dynabeads (Chromotek) for each sample were washed with ice-cold lysis buffer 3x and collected by spinning at 550 g for 1 min at 4 °C. Buffer was carefully removed using a pipette on a magnetic rack to avoid loss of beads. Beads were then blocked using 1 ml lysis buffer with 50 µg yeast tRNA (Thermo Fisher Scientific) for 1 h at 4 °C with slow rotation. Blocking buffer was removed and beads were again washed with ice-cold lysis buffer 3x. 200 µl clarified cell lysates were added to each tube containing blocked-beads and slowly rotated for 2 h at 4 °C. 50ul lysate was kept aside for any further analysis. Half of the bead suspension (100 µl) was transferred to a new Eppendorf tube and fixed using 5 mM reversible cross-linker DSP (dithiobis[succinimidylpropionate]) (Thermo Fisher Scientific) for 30 min at 4 °C with slow rotation. After fixation, both fixed and un-fixed beads were washed 4x using 1 ml lysis buffer with 1 µl RNaseout and 2 µl protease and phosphatase inhibitor.10% samples were taken for silver staining (Quality control) in 10ul lysis buffer (and kept at 4 °C), 1% sample for confocal imaging, and rest of the bead samples kept in 20 µl lysis buffer at 4 °C for quantitative mass spectrometry.

LC-MS Analysis. G45 nuclear body samples were analyzed as previously described(5). Briefly, proteins were digested using the Strap (protifi.com) per the manufacturer's instructions. Resulting peptides were analyzed by nanoLC MS/MS using an Aurora C18 column (IonOpticks)coupled to an Orbitrap Eclipse (Thermo) with a 120 min gradient and data dependent acquisition. MS1 and MS2 scans were acquired at resolutions of 120,000 and 15,000, respectively, using stepped HCD fragmentation. Data were searched against the Human proteome using Proteome Discoverer, applying standard mass tolerances, carbamidomethylation as a fixed modification.

RNA-Seq. RNA-Seq was performed at the MD Anderson Cancer Center Advanced Technology Genomics Core (ATGC). Barcoded, Illumina compatible, stranded total RNA libraries were prepared using the Illumina Stranded Total RNA Prep Ligation with Ribo-Zero Plus Kit (Illumina). Briefly, 100ng of DNase I treated total RNA was depleted of cytoplasmic and mitochondrial ribosomal RNA (rRNA) using Ribo-Zero Plus. The remaining ribosomal depleted RNA was fragmented and reverse transcribed using random hexamers. Deoxyuridine triphosphate (dUTP) was incorporated during second strand synthesis to provide strand specificity. The ends of the resultant double stranded cDNA fragments were repaired, 3'-A tailed, then pre-index anchors were ligated. The products were then purified, and Illumina specific dual indexes added using 13

cycles of PCR, to create the final cDNA library. The libraries were quantified using the Qubit dsDNA HS Assay Kit and assessed for size distribution using the Agilent Tapestation (Agilent Technologies), then pooled. The pools were quantified by qPCR using the KAPA Library Quantification Kit (Kapa Biosystems). Each library pool was then sequenced on an Illumina NovaSeq6000 SP-200 flow cell (R1121) using the 100nt PE format. The raw data of total RNA-Seq (GSE324180) for this study have been deposited in the NCBI's Gene Expression Omnibus (GEO) database.

ChIP-Seq. These assays were performed at the MD Anderson Cancer Center Epigenomics Profiling Core following the protocol as described previously (6, 7) with some modifications. Briefly, 10 million cells were crosslinked in 1% formaldehyde for 12 min, followed by incubation with 125mM glycine for 5 min at RT. Chromatin was prepared by nuclear isolation followed by lysis. Lysates were subjected to sonication with a Bioruptor Pico (Diagenode) to obtain DNA fragments ranging from 200-600 bp followed by centrifugation at 16,000g for 10 min at 4°C. The supernatant containing chromatin lysate was pre-cleared with DynabeadsTM Protein A beads (Invitrogen) for 1 h at 4°C, and incubated with BLZF1 antibody (Aviva) conjugated with DynabeadsTM Protein A beads (Invitrogen) overnight at 4°C. Next day, beads were collected using DynaMag-2 magnet (Invitrogen), washed extensively, and ChIP DNA isolated after reversing the crosslinks. Input and ChIP DNA libraries were prepared using NEBNext® Ultra™ II DNA Library Prep Kit for Illumina® (New England Biolabs, Ipswich, MA) following manufacturer's instructions and submitted for sequencing on an Illumina NovaSeq 6000 to obtain at least 30 million high quality mapping reads per sample. The raw data for this study have been deposited in the NCBI's Gene Expression Omnibus (GEO) database (GSE324179).

ATAC-Seq. ATAC-Seq assay and libraries were prepared at the MD Anderson Epigenomics Profiling Core following the protocol as previously described(8) with minor modifications. Briefly, 50,000 nuclei (isolated from 1 x 10^5 cells) were incubated with Tagment DNA TDE1 enzyme (Illumina), followed by DNA purification and library preparation. The resulting libraries were sequenced 2 x 75 bp on an Illumina NextSeq500 to obtain, on average, 89.6 million high quality mapping reads per sample. The raw data for this study have been deposited in the NCBI's Gene Expression Omnibus (GEO) database (GSE324178).

Biotinylated DNA pull-down assay. Biotinylated and non-biotinylated DNA oligonucleotides were synthesized by MilliporeSigma and annealed to generate double-stranded DNA (dsDNA). For DNA pull-down assays, 50-bp 5′-biotinylated dsDNA probes containing AP-1 binding sites derived from the SPP1 promoter at positions −198 bp or −81 bp were used. A 50-bp dsDNA fragment derived from EGFP served as a negative control. DsDNA sequences are provided in Supplemental Table 6. DNA pull-down assays were performed as previously described(9) with minor modifications. Briefly, 500 µg of nuclear extracts from DKO or DKO cells stably expressing HA-tagged G45 were adjusted to 150 mM NaCl and incubated with 200 pmol biotinylated dsDNA overnight at 4 °C. For competition assays, 1 µmol of corresponding non-biotinylated dsDNA was included in the reaction. Following incubation, 40 µL of high-capacity streptavidin-agarose beads (Thermo Fisher Scientific) were added and the mixture was further incubated for 2 h at 4 °C. Beads were collected by centrifugation (4,000 rpm, 1 min), washed four times with 1× RIPA buffer,

and bound proteins were eluted by boiling in 1× SDS loading buffer for 10 min. The resulting samples were subjected to Western blot analysis.

GST-G45 protein purification. HEK293T cells were transfected with a GST-G45 expression plasmid and harvested 48 h post-transfection. Cells were lysed in 1× RIPA buffer, and the lysates were mixed 1:1 with equilibration/wash buffer (125 mM Tris-HCl, 150 mM NaCl, 1 mM DTT, 1 mM EDTA, pH 7.4). The mixture was incubated with Pierce glutathione magnetic agarose beads (Thermo Fisher Scientific) on an end-over-end rotator for 2 h at 4 °C. Following incubation, beads were collected using a magnetic stand and washed four times with equilibration/wash buffer. Bound proteins were eluted by incubation with 500 µL elution buffer (50 mM reduced glutathione in equilibration/wash buffer, pH 7.4) for 20 min at RT. The eluates were concentrated using Amicon Ultra centrifugal filters (10 kDa MWCO; MilliporeSigma), supplemented with 10% glycerol, aliquoted, flash-frozen in liquid nitrogen, and stored at −80 °C.

Electrophoretic mobility shift assays. The Gelshift Chemiluminescent EMSA Kit (Active Motif) or the LightShift Chemiluminescent EMSA Kit (Thermo Fisher Scientific) were utilized according to the manufacturers' instructions. Briefly, biotin-labeled DNA probes were incubated with purified proteins at RT for 20 min. The binding reactions were then resolved on a 6% native polyacrylamide gel and subsequently transferred onto a nylon membrane. DNA–protein complexes were crosslinked to the membrane using a UV crosslinker. Membranes were blocked for 15 min and incubated with streptavidin–HRP conjugate for 15 min, followed by four washes. Signals were detected using a chemiluminescent substrate and visualized with a ChemiDoc imaging system (Bio-Rad). Promoter oligonucleotides utilized for EMSA are identical to those utilized for Biotinylated DNA pull-down assay.

Statistics. For RNA-seq, raw reads were aligned to human genome and transcriptome (reference genome GRCh38) using RSEM v1.3.3 (10) with bowtie2 v 2.4.2(11) and default parameters. The reads count for each gene were estimated and normalized to TPM values (tag per million reads). Differential gene expression analyses were performed using EdgeR package (v3.32.1) (12). Differential genes between treatment and control groups were identified at FDR cutoff 0.01 and absolute log2 fold change > 1. The gene set enrichment analysis was performed using GSEA suite v4.4.0 (13). The GO term analysis was performed using DAVID v2025_2 (14). All plots were generated using in-house R scripts. For ATAC-seq and ChIP-seq, raw reads were aligned to human genome (GRCh38) using BWA v 0.7.16a-r1181 (15) and sorted using SAMTOOLS v1.19 (16). Reads piling and peak calling were performed using MACS2 v2.1.1 (17) with adjusted p-value cutoff 1e-4 and rest default parameters. The peak profiles were converted into UCSC WIG format for visualization in UCSC genome browser (http://genome.ucsc.edu). The peak regions across the replicates were merged and aligned to create an aligned reference peak file using BEDTOOLS v2.27.1 (18). The peak files were annotated using HOMER v4.8 (19) for genomic features. Peaks were associated with genes within promoter regions or gene bodies, or in nearest intergenic regions. The gene level results were combined with RNA-seq results for subset and integrated analyses. All plots were generated using in-house R scripts.

For proteomic analysis on G45 bodies, we utilized unfixed and DSP-fixed conditions to identify proteins that increased in abundance upon fixation. Using the LC-MS normalized abundance

data, a protein was considered to be associated with the DSP-fixed EGFP-tagged G45 body if it was enriched at least 2-fold compared to: (1) unfixed EGFP control; (2) DSP-fixed EGFP control; and (3) unfixed EGFP-G45.

Unless otherwise indicated, data are presented as the mean ± SD from at least two independent experiments or from randomly selected cells within a field. Statistical analyses were performed using Prism 10 (GraphPad Software). Comparisons between two groups were conducted using unpaired, two-tailed Student's t tests, while multiple group comparisons were performed using one-way ANOVA followed by Tukey's post hoc test. A P value < 0.05 was considered statistically significant.

References

1. Tan X, Shi L, Banerjee P, Liu X, Guo HF, Yu J, et al. A protumorigenic secretory pathway activated by p53 deficiency in lung adenocarcinoma. *J Clin Invest*. 2021;131(1).
2. Mi W, Guan H, Lyu J, Zhao D, Xi Y, Jiang S, et al. YEATS2 links histone acetylation to tumorigenesis of non-small cell lung cancer. *Nature communications*. 2017;8(1):1088.
3. Tang F, Xu D, Wang S, Wong CK, Martinez-Fundichely A, Lee CJ, et al. Chromatin profiles classify castration-resistant prostate cancers suggesting therapeutic targets. *Science*. 2022;376(6596):eabe1505.
4. Kumar A, Tanaka K, and Schwartz MA. Focal adhesion-derived liquid-liquid phase separations regulate mRNA translation. *Elife*. 2025;13.
5. Wang S, Guo H, Fukushima R, Terajima M, Liu M, Xiao GY, et al. Lysyl hydroxylase 2 glucosylates collagen VI to drive lung cancer progression. *J Clin Invest*. 2025;135(7).
6. Jain AK, Xi Y, McCarthy R, Allton K, Akdemir KC, Patel LR, et al. LncPRESS1 Is a p53-Regulated LncRNA that Safeguards Pluripotency by Disrupting SIRT6-Mediated De-acetylation of Histone H3K56. *Mol Cell*. 2016;64(5):967–81.
7. Mahadevan KK, LeBleu VS, Ramirez EV, Chen Y, Li B, Sockwell AM, et al. Elimination of oncogenic KRAS in genetic mouse models eradicates pancreatic cancer by inducing FAS-dependent apoptosis by CD8(+) T cells. *Dev Cell*. 2023;58(17):1562–77 e8.
8. Corces MR, Trevino AE, Hamilton EG, Greenside PG, Sinnott-Armstrong NA, Vesuna S, et al. An improved ATAC-seq protocol reduces background and enables interrogation of frozen tissues. *Nat Methods*. 2017;14(10):959–62.
9. Tsuji Y. Optimization of Biotinylated RNA or DNA Pull-Down Assays for Detection of Binding Proteins: Examples of IRP1, IRP2, HuR, AUF1, and Nrf2. *Int J Mol Sci*. 2023;24(4).
10. Li B, and Dewey CN. RSEM: accurate transcript quantification from RNA-Seq data with or without a reference genome. *BMC Bioinformatics*. 2011;12:323.
11. Langmead B, and Salzberg SL. Fast gapped-read alignment with Bowtie 2. *Nat Methods*. 2012;9(4):357–9.

12. Robinson MD, McCarthy DJ, and Smyth GK. edgeR: a Bioconductor package for differential expression analysis of digital gene expression data. *Bioinformatics*. 2010;26(1):139–40.
13. Subramanian A, Tamayo P, Mootha VK, Mukherjee S, Ebert BL, Gillette MA, et al. Gene set enrichment analysis: a knowledge-based approach for interpreting genome-wide expression profiles. *Proc Natl Acad Sci U S A*. 2005;102(43):15545–50.
14. Sherman BT, Hao M, Qiu J, Jiao X, Baseler MW, Lane HC, et al. DAVID: a web server for functional enrichment analysis and functional annotation of gene lists (2021 update). *Nucleic Acids Res*. 2022;50(W1):W216–W21.
15. Li H, and Durbin R. Fast and accurate short read alignment with Burrows-Wheeler transform. *Bioinformatics*. 2009;25(14):1754–60.
16. Li H, Handsaker B, Wysoker A, Fennell T, Ruan J, Homer N, et al. The Sequence Alignment/Map format and SAMtools. *Bioinformatics*. 2009;25(16):2078–9.
17. Feng J, Liu T, Qin B, Zhang Y, and Liu XS. Identifying ChIP-seq enrichment using MACS. *Nat Protoc*. 2012;7(9):1728–40.
18. Quinlan AR, and Hall IM. BEDTools: a flexible suite of utilities for comparing genomic features. *Bioinformatics*. 2010;26(6):841–2.
19. Zhang F, and Chen JY. HOMER: a human organ-specific molecular electronic repository. *BMC Bioinformatics*. 2011;12 Suppl 10(Suppl 10):S4.